Cell, Vol. 115, 97–108, October 3, 2003, Copyright ©2003 by Cell Press

Structure of the Mammalian Mitochondrial Ribosome Reveals an Expanded Functional Role for Its Component Proteins

Manjuli R. Sharma,[1] Emine C. Koc,[2] Partha P. Datta,[1] Timothy M. Booth,[1] Linda L. Spremulli,[2] and Rajendra K. Agrawal[1,3,*]

[1]Division of Molecular Medicine
Wadsworth Center
New York State Department of Health
Empire State Plaza
Albany, New York 12201

[2]Department of Chemistry
Campus Box 3290
University of North Carolina
Chapel Hill, North Carolina 27599

[3]Department of Biomedical Sciences
State University of New York at Albany
Albany, New York 12222

Summary

The mitochondrial ribosome is responsible for the biosynthesis of protein components crucial to the generation of ATP in the eukaryotic cell. Because the protein:RNA ratio in the mitochondrial ribosome (~69:~31) is the inverse of that of its prokaryotic counterpart (~33:~67), it was thought that the additional and/or larger proteins of the mitochondrial ribosome must compensate for the shortened rRNAs. Here, we present a three-dimensional cryo-electron microscopic map of the mammalian mitochondrial 55S ribosome carrying a tRNA at its P site, and we find that instead, many of the proteins occupy new positions in the ribosome. Furthermore, unlike cytoplasmic ribosomes, the mitochondrial ribosome possesses intersubunit bridges composed largely of proteins; it has a gatelike structure at its mRNA entrance, perhaps involved in recruiting unique mitochondrial mRNAs; and it has a polypeptide exit tunnel that allows access to the solvent before the exit site, suggesting a unique nascent-polypeptide exit mechanism.

Introduction

The mammalian mitochondrial ribosome (mitoribosome) is responsible for the synthesis of 13 proteins of the inner mitochondrial membrane. These proteins are components of the oligomeric complexes essential for oxidative phosphorylation (Attardi, 1985; Chomyn et al., 1986). Thus, mitoribosomes synthesize crucial cellular components needed to generate about 90% of the ATP required by a eukaryotic cell. Although the role of mitochondria in apoptosis is well documented (Brenner and Kroener, 2000), recent identification of the two death-associated proteins DAP3 and PDCD9 as mitochondrial ribosomal proteins (Koc et al., 2001a) indicates that mitoribosomes play a direct role in apoptosis. According to several genomic analyses, mitochondria are believed to have arisen from an early endosymbiotic event between a eubacterium and its host cell (e.g., Gray et al., 2001), and the closest free-living relatives of mitochondria are members of the rickettsial subdivision of the α-proteobacteria. Therefore, it has generally been expected that the mitoribosome will display greater structural and functional similarities to a bacterial ribosome than to a eukaryotic cytoplasmic ribosome.

Like all ribosomes, the bovine 55S mitoribosome (molecular mass 2.71 MDa) consists of two multicomponent and unequally sized subunits: small (28S) and large (39S) (O'Brien, 1971). However, the RNA and protein composition of the mitoribosome differs significantly from that of bacterial ribosomes (also see O'Brien, 2002). The 28S small subunit (SSU) contains a 12S rRNA (950 nucleotides) and 29 proteins (Koc et al., 2000; O'Brien et al., 2000; Suzuki et al., 2001a), in contrast to its widely studied bacterial 30S counterpart, which is composed of a 16S rRNA (1542 nucleotides) and 21 proteins (numbered S1–S21) (Wittmann-Liebold, 1985). The 39S large subunit (LSU) of the mitoribosome contains a 16S rRNA (1560 nucleotides) and 48 proteins (Koc et al., 2001b; O'Brien et al., 2000; Suzuki et al., 2001b), while its bacterial 50S counterpart is composed of two rRNA molecules (5S, 120 nucleotides; 23S, 2904 nucleotides) and 33 proteins (numbered L1–L36) (Wittmann-Liebold, 1985). Thus, the protein-to-RNA ratio is completely reversed in the mitoribosome (69% protein and 31% RNA) relative to bacterial ribosomes (33% protein and 67% RNA). The mitoribosomal rRNAs are significantly shortened through the loss of specific secondary structural elements. Among the 77 component proteins of the mitoribosome, almost half are mitoribosome-specific proteins, while the rest are homologs of bacterial proteins. The homolog proteins in the mitoribosome are usually significantly larger than the corresponding bacterial proteins (O'Brien, 2002). Recent studies have indicated that homolog proteins found near the binding sites of truncated rRNA regions are significantly larger than the corresponding proteins in the bacterial ribosome; this pattern suggests the mitoribosome's structural and functional compensation of such truncated rRNA segments through increases in the size of these homolog proteins (Suzuki et al., 2001a, 2001b). Despite its greater molecular mass (2.71 MDa), the mitoribosome has a lower sedimentation coefficient (55S) than the bacterial 70S ribosome (2.3 MDa). This, taken with other physiochemical findings (Patel et al., 2001), suggests that the mitoribosome has a larger physical size but a more porous structure than its bacterial counterpart.

Here, we present a 13.5 Å resolution (9.1 Å by the 3σ criterion; Orlova et al.,1997) cryo-EM structure of the bovine 55S mitoribosome carrying a mitochondrial tRNA (mt tRNA) bound at its P site. The map reveals several distinctive features that have not been seen in the cryo-EM maps of cytoplasmic ribosomes from prokaryotic (Gabashvili et al., 2000) or eukaryotic (Dube et al., 1998; Spahn et al., 2001) organisms. Molecular analysis of the cryo-EM map, by computational separation of the ribosomal RNA and protein components (Spahn et al., 2000) and by comparison to the X-ray structures of the

*Correspondence: agrawal@wadsworth.org

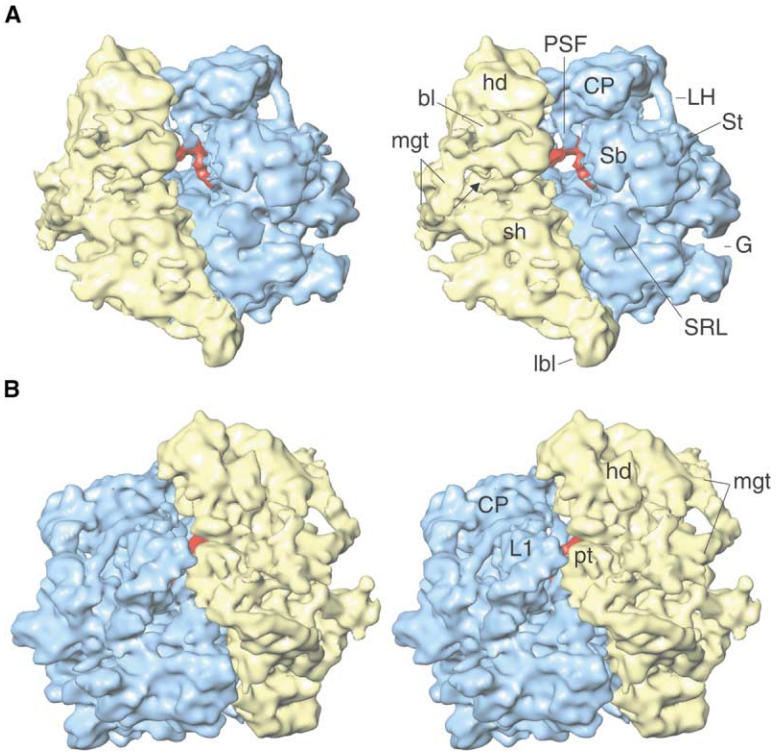

Figure 1. Stereo Representation of the Cryo-EM Structure of the Bovine 55S Mitoribosome

(A) A side-by-side view showing the shoulder (sh) side of the 28S small subunit (SSU, yellow) and the L7/12 protein-stalk (St) side of the 39S large subunit (LSU, blue). A density (red) corresponding to the P site bound mt tRNA bridges the intersubunit space.

(B) Another side-by-side view, in which the mitoribosome has been rotated by ~180° around a virtually vertical axis, shows the platform (pt) side of the SSU and L1-protein (L1) side of the LSU. The two subunits (SSU and LSU) and the mt tRNA were computationally differentiated. Landmarks of the SSU: hd, head; bl, beak lobe; mgt, mRNA-entry gate; lbl, lower-body lobe. The arrow in (A) points to the mRNA entrance. Landmarks of the LSU: CP, central protuberance; Sb, stalk base; SRL, α-sarcin-ricin loop; PSF, P site finger; LH, LSU handle; G, a gap originating principally through the absence of domain I in LSU rRNA (see Figures 5A and 5E).

mitoribosome's closest relatives, the bacterial ribosomes (Ban et al., 2000; Harms et al., 2001; Wimberly et al., 2000; Yusupov et al., 2001), provides new insights into the structural and functional evolution of the mitoribosome.

Results and Discussion

Structure of the 55S Mitoribosome

The cryo-EM map of the bovine 55S mitoribosome (Figure 1) reveals a porous structure with a few large masses protruding from the main, relatively compact and globular core. The diameter of the mitoribosome is ~320 Å (in the direction of the longest axis), about 60 Å larger than the bacterial 70S ribosome (also see Supplemental Figure S1A online at http:///www.cell.com/cgi/content/full/115/1/97/DC1). While characteristic structural features for both ribosomal subunits (for example, body, head, and platform of the SSU and the L1- and L7/L12-stalks and central protuberance [CP] of the LSU) are immediately recognized in the cryo-EM map, the overall structural organization in both subunits is markedly divergent from that of other ribosomes. The two subunits of the mitoribosome enclose an intersubunit space that has an overall similarity to its cytoplasmic counterparts. However, the factor binding region of this intersubunit space, along the margin of the two subunits, is distinctly different from and has a relatively more open configuration than that in cytoplasmic ribosomes (Stark et al., 1997; Agrawal et al., 1998; Gomez-Lorenzo et al., 2000; Valle et al., 2002). Furthermore, a finger-like structure (described later) extends from the CP of the LSU into the intersubunit space.

We have computationally separated the RNA and protein components within both subunits of the mitoribosome (Figure 2) based on differential scattering properties of the two ribonucleoprotein components, as estimated from density histogram information and by using a technique of "region growing" (Spahn et al., 2000). The map reveals that the major portion of the rRNA component of the mitoribosome is heavily shielded by peripheral protein masses (also see Supplemental Movie S1). This situation is strikingly different from that in the bacterial ribosome (Ban et al., 2000); in the latter, proteins decorate the periphery only in discrete patches. Regions of the mitoribosome map classified as rRNA show signatures of major grooves and, in some places, minor grooves, characteristic of the double-stranded segments of the rRNAs (see, for example, helix 44, Figure 2C). The regions classified as rRNA correspond well with the rRNA domains known to be conserved between the mitoribosome and bacterial ribosomes based on the X-ray structures of the bacterial ribosomes (Ban et al., 2000; Harms et al., 2001; Wimberly et al., 2000), except for a small region (marked with an asterisk in Figure 2C) that lies close to the decoding site in the SSU. This region may correspond to a bound segment of mitochondrial mRNA.

Intersubunit Bridges

We have analyzed the contact points between the two mitoribosomal subunits using the map in which the rRNA and protein components have been separated. The two subunits are held together by 15 intersubunit bridges (Figures 2C and 2D), of which six (B2a–B2c, B3, B5, and B7a) are conserved and have chemical compositions similar to their counterparts in bacterial ribosomes (Yusupov et al., 2001). The other nine bridges all involve

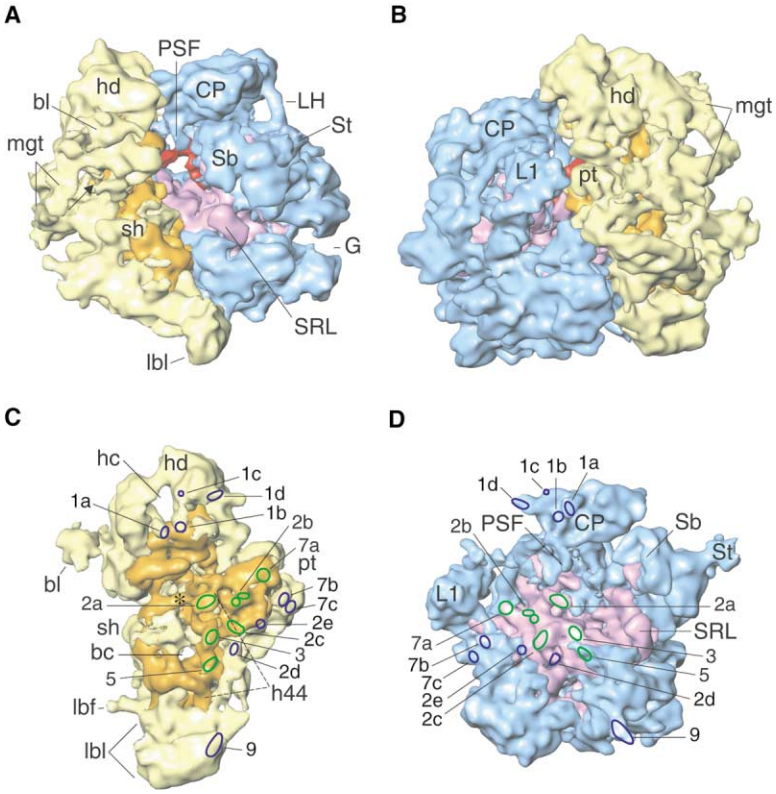

Figure 2. Separation of rRNA and Protein Components of the Mitoribosome and Locations of the Intersubunit Bridges

(A and B) The 55S ribosome map in which the RNA (orange in the SSU and purple in the LSU) and protein (yellow in the SSU and blue in the LSU) moieties have been separated is shown in views similar to those in Figure 1. The SSU (C) and LSU (D) are shown from their interface sides to reveal intersubunit bridges. The asterisk in (C) points to a density near the decoding site of the SSU that is classified as an rRNA segment but is not filled by any rRNA segment in the X-ray structure of the bacterial SSU. Locations of the 15 intersubunit bridges have been marked on both subunits as ellipses: green for conserved bridges and dark blue for mitoribosome-specific bridges. Each bridge is identified by a number-letter combination. Landmarks: hc, head channel; bc, body channel; h44, rRNA helix 44 (see Figure 3A for rRNA helix identifications); lbf, lower-body finger. All other landmarks are as in Figure 1.

protein and differ from the bacterial bridges in either spatial position or chemical composition. Among the nine mitoribosome-specific bridges, four (B1a–B1d) correspond to the bacterial B1 bridge group (here, group denotes the general location of bridges, following the nomenclature used for the bacterial ribosome [Gabashvili et al., 2000; Yusupov et al., 2001]). Accordingly, the other four bridges are denoted as B2d, B2e, B7b, and B7c. The ninth bridge, B9, which connects the lowermost regions of the LSU and SSU, occupies a position that has no bacterial counterpart. In summary, the mitoribosomal subunits are held together by five RNA-RNA bridges, two RNA-protein bridges, seven protein-protein bridges, and one bridge that involves both RNA and protein components from both subunits (Figures 2C and 2D). Thus, in contrast to cytoplasmic ribosomes in which the majority of bridges are RNA-RNA (Spahn et al., 2001; Yusupov et al., 2001), the mitoribosome is dominated by protein-protein bridges. The decrease in the number of RNA-RNA bridges reflects the truncation of several rRNA helices in the mitoribosome (see below). These observations indicate that during the evolution of the mitoribosome, proteins took over some of the functions of rRNAs, including much of their participation in the intersubunit communication.

Structure of the Mitoribosomal Small Subunit

The 28S SSU of the mitoribosome is much more elongated (by ~70 Å) than its bacterial 30S counterpart, but it is significantly narrower (by ~15 Å) in its midbody region. The head of the mitoribosomal SSU is enlarged and displays a peculiar, obliquely oriented channel that connects the interface side of the subunit with the solvent (Figures 2C and 3B). Of the head, body, and platform regions of the SSU, the platform is the most strongly conserved structural component (Figure 3B). Significant amounts of additional protein mass are present in the head and in the lower-body region of the mitoribosomal SSU.

Comparison of the secondary structure diagrams of the mitoribosome 12S rRNA and of the bacterial 16S rRNA (Cannone et al., 2002; Figure 3A) shows that the 16S rRNA helices 6, 8–10, 12, 13, 16, 17, 21, 26, 33, 37, and 39–41, as well as the rRNA segment bearing the anti-Shine-Dalgarno sequence, are absent in the mitoribosomal rRNA. In addition, several other rRNA helices are shorter. These characteristics of the rRNA secondary structure are reflected in the higher-order structural features seen in our cryo-EM map. This allows us to dock accurately the conserved rRNA portions and proteins of the bacterial SSU's crystallographic structure (Wimberly et al., 2000) into the cryo-EM map of the mitoribosome SSU (Figures 3B and 3C). The crystallographic structure fits almost as a rigid body, requiring only small adjustments in the relative positions of the main body, head, and platform regions.

The mitoribosomal SSU lacks the beaklike feature of the head (however, see below), and its shoulder is narrowed. This morphology is consistent with the absence of helices 33 and 33a, and helices 16 and 17, respectively, in the mitoribosome (Figure 3D): it indicates that these and many other RNA segments are not replaced by any protein mass. Due to the absence of helices 16 and 17, the factor binding region between the two mitoribosomal subunits is more open. The absence of helices 12 and 21 creates a channel almost in the center

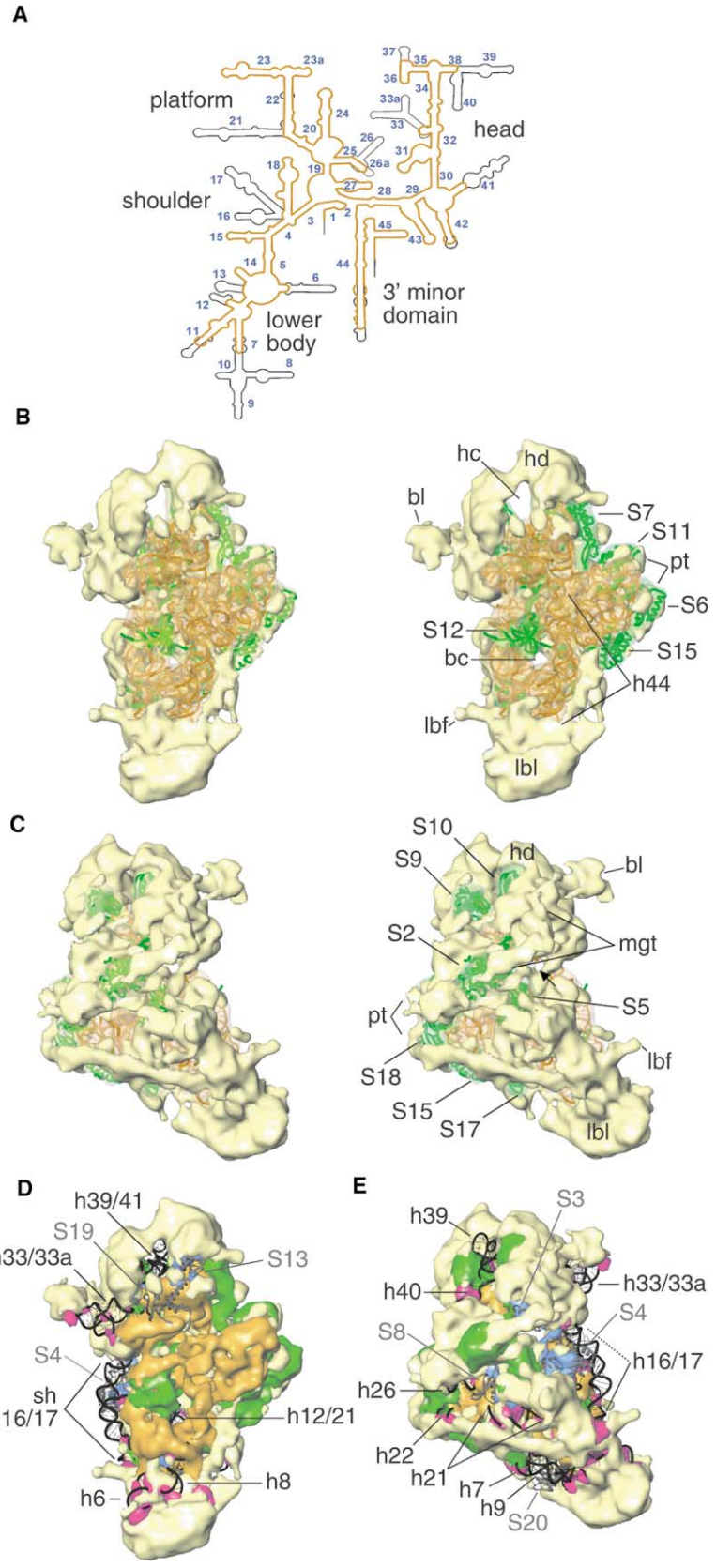

Figure 3. Structural Analysis of the SSU of the Mitoribosome

(A) Secondary structure diagram of the bovine mitochondrial 12S rRNA (orange), superimposed on that of the bacterial 16S rRNA. RNA regions absent in the mitoribosome thus appear black. RNA helices are identified by the adjacent numbers.

(B) Stereo representation of the fitting of the conserved domains (ribbons) from the crystallographic structure of the *Thermus thermophilus* 30S SSU (Wimberly et al., 2000; PDB ID 1FJF) into the cryo-EM map of the mitoribosome SSU, shown from its interface side. The conserved structural components (orange, rRNA; green, homologous proteins) are shown as translucent surfaces, while the mitoribosome-specific proteins are shown as solid yellow surfaces.

(C) Stereo representation of the fitting, shown from an oblique, solvent-side view. The arrow points to the mRNA-entry site.

(D and E) Superposition of the nonconserved domains from the crystallographic structure of the bacterial SSU (black ribbons, rRNA; gray ribbons, proteins) onto the mitoribosomal SSU map (solid surfaces) shown in views similar to those in (B) and (C). Small patches colored in magenta and blue correspond, respectively, to protein masses that compensate for missing segments of bacterial rRNA and proteins, (also see Supplemental Figure S1B). Thus, the yellow regions in (D) and (E) represent the protein masses that do not compensate for any missing bacterial ribosomal components. Landmarks: Numbers prefixed "S" represent the SSU proteins; numbers prefixed "h" identify the rRNA helices. All other landmarks are as in Figures 1 and 2.

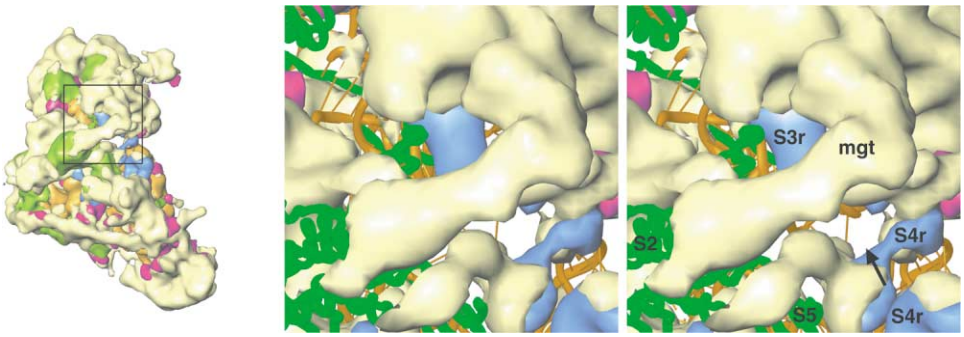

Figure 4. Stereo Representation of the Detailed Topography of the mRNA Entry Site

The site is composed principally of proteins and is partially covered by a triangular gatelike structure (mgt), which is composed of mitoribosome-specific proteins (yellow). The conserved SSU proteins (green) S2 and S5 and mitoribosome-specific protein masses (blue) that replace bacterial protein S3 and segments of protein S4 are identified with the suffix r. The panel on the left shows the orientation (similar to that in Figures 3C and 3E) of the 28S SSU; the boxed area has been enlarged for the stereo depiction.

of the main body, while the absence of helices 39 and 41 results in a channel in the head region (Figures 3B and 3D). Helix 6, which forms the spur of the bacterial SSU (Wimberly et al., 2000), is absent in the mitoribosome; however, a finger-like protein protrusion (lower-body finger, or lbf in Figures 1–3) is situated in the same general area, perhaps compensating for the spur's absence. One of the longest helices of the bacterial SSU rRNA that is absent in the mitoribosome is helix 21. This helix is partially replaced in the mitoribosome by protein (Figure 3E). In addition, an elongate protein mass, which spans the platform and the main body on the solvent side and which parallels the position of the missing helix 21, is present in the mitoribosome. Helix 10, which is present in the lower-body region of the bacterial SSU but missing in the mitoribosomal SSU, is fully compensated by proteins in the latter. Altogether, only ~19% of the missing bacterial SSU rRNA segments are replaced, in small patches, by proteins in the mitoribosomal SSU (Figures 3D and 3E, also see Supplemental Figure S1B). The lower-body portion of the SSU is composed of a complex mass of proteins, which we term the lower-body lobe (lbl in Figures 1–3).

Fourteen of the mitoribosome proteins, S2, S5–S7, S9–S12, S14–S18, and S21, are known to have significant sequence homology with their bacterial counterparts; however, they are each 4–25 kDa larger than the corresponding bacterial proteins, except for proteins S6 and S12, which are actually shorter in the mitoribosome (Koc et al., 2000; Suzuki et al., 2001a). Bacterial proteins S3, S4, S8, S13, S19, and S20 are known to be absent in the mitoribosome. Interestingly, S4, S8, and S20 are primary RNA binding proteins, and S13 in the bacterial ribosome is involved in the formation of two intersubunit bridges (bridges B1a and B1b) with the LSU (Yusupov et al., 2001). The configurations of these two bridges alter during EF-G-dependent translocation in the bacterial ribosome (Frank and Agrawal, 2000, 2001). Apparently, the role of S13 is taken over here by mitoribosome-specific proteins, which form four distinct bridges (B1a–B1d) with the CP of the LSU (Figures 2C and 2D). However, only a small portion of the N-terminal domain of S13 is replaced by mitoribosome-specific protein (Figure 3D). The positions of proteins S19 and S20 and a major portion of protein S8 (the status of S3 and S4 is described below) remain unfilled in the mitoribosome. A large globular protein structure emerges from the solvent side of the head and extends toward the region that would, in the bacterial ribosome, be occupied by the tip of the beaklike structure formed by helix 33a (Figure 3D). We designate this structure the beak lobe (bl in Figures 1A, 2A, 2C, and 3).

The mRNA Entrance Site

One of the most striking structural features of the mitoribosome SSU is a triangular gatelike structure (termed the mRNA gate or mgt in Figures 1, 2A, 2B, and 3C) that partially covers the mRNA entry site (see Frank et al., 1995). This large structure (Figure 4) is apparently formed by an extension of protein S2 (which is larger in the mitoribosome) and by a protein situated on the solvent side of the SSU head (also see Supplemental Movie S1). In the bacterial ribosome, the entrance of the mRNA channel is surrounded by ribosomal proteins S3, S4, and S5 (Yusupova et al., 2001). Two of these, proteins S3 and S4, are absent in the mitoribosome. While the position of protein S3 is almost completely filled by mitoribosome-specific proteins, the position of S4 is only partially filled (Figures 3D and 3E), mainly in the segments of S4 that encircle the mRNA entrance (Figure 4). Despite the absence of bacterial proteins S3 and S4, the composition of the mRNA entrance is predominantly protein.

The mitoribosome synthesizes 13 polypeptide chains from nine monocistronic and two dicistronic mRNAs with overlapping reading frames (Anderson et al., 1982; Wolstenholme, 1992). The mitochondrial mRNAs (mt mRNAs) show an almost complete lack of the 5′ and 3′ untranslated regions that are characteristic of bacteria (e.g., the Shine-Dalgarno sequence) and eukaryotes (the 5′ cap). In the mt mRNAs, the start codon is generally located within three nucleotides of the 5′ end (Anderson et al., 1982; Ojala et al., 1980). It is likely that the mitoribosome has evolved specific features to recognize its unusual mRNAs. The strategic location of the mRNA gate suggests that this structure could be involved in the regulation of translation initiation, perhaps by aiding in the recruitment of the mt mRNAs to the SSU.

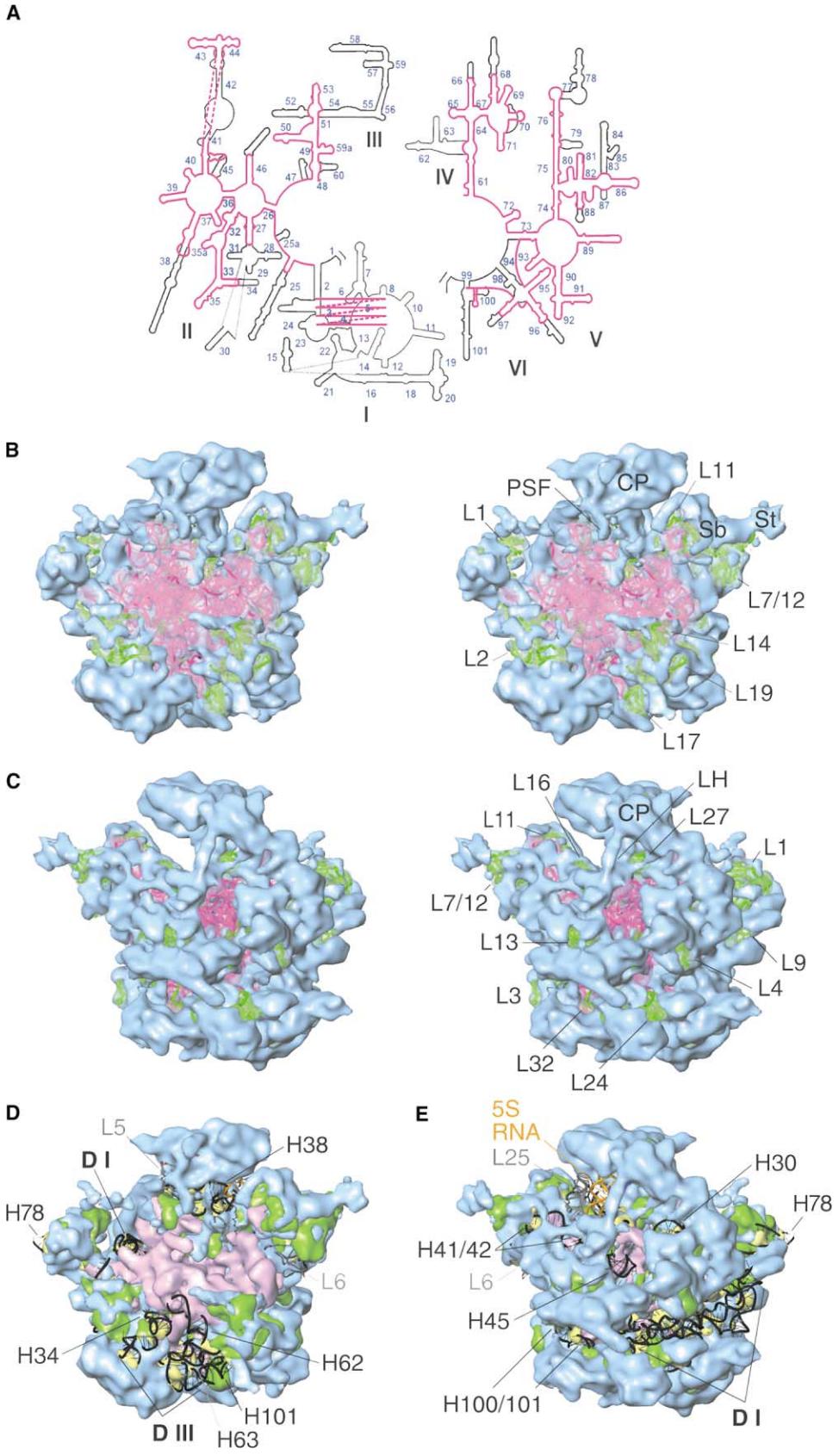
A
I
II
III
IV
V
VI
B
PSF
CP
L11
L1
Sb
St
L7/12
L14
L2
L19
L17
C
L16
LH
L11
CP
L27
L1
L7/12
L13
L9
L4
L3
L32
L24
D
L5
H38
D I
H78
L6
H34
H62
H101
D III
H63
E
5S
RNA
L25
H30
H78
H41/42
L6
H45
H100/101
D I

Structure of the Mitoribosomal Large Subunit

Like the SSU, the 39S LSU of the mitoribosome is larger than its bacterial counterpart, and all three of the distinctive LSU structural features, namely the L7/L12 stalk, CP, and L1 stalk, are correspondingly larger. A comparison of the secondary structures of the 16S rRNA of the mitoribosomal LSU and the 23S rRNA of the bacterial LSU (Cannone et al., 2002) reveals a number of bacterial rRNA segments that are absent in the mitoribosome (Figure 5A). Among the six recognized secondary structure domains of the bacterial 23S RNA, domain I is almost completely absent in the mitoribosome, a fact immediately deducible from our cryo-EM map (gap or G in Figure 1A). A significant portion of domain III is also absent. Our map shows that most of the missing segments of domain I are left unfilled (Figure 5E), while those of domain III are partially compensated by proteins (Figure 5D).

Strikingly, the 23S rRNA helix 38, which in the bacterial ribosome forms one of the RNA-protein intersubunit bridges (bridge B1a) with the SSU and which also makes important contacts with both A and P site tRNAs (Yusupov et al., 2001), is truncated in the mitoribosome. That bacterial RNA-protein bridge is replaced by a protein-protein bridge in the analogous region of the mitoribosome. Other LSU rRNA helices that are absent or shorter in the mitoribosome yet are known to be involved in the formation of intersubunit bridges in the bacterial ribosome include helices 34 (bridge B4), 62 (bridges B5 and B6), and 68 (bridge B7a). Despite the truncations of these rRNA helices, the overall structural organization of bridges B5 and B7a appears to be preserved in the mitoribosome. While the configuration of bridge B4 (here designated as B2e) has changed significantly in the mitoribosome, bridge B6 is absent altogether here.

Ribosomal RNA helices 77 and 78 (domain V), which form the major portion of the L1 stalk in the bacterial ribosome (Yusupov et al., 2001, Harms et al., 2001), are absent in the mitoribosome. Structurally, they are almost completely replaced by proteins (Figures 2B, 2D, 5D, and 5E), suggesting that the function of rRNA is entirely taken over by the much larger L1 homolog and other proteins in this region of the mitoribosome (see Suzuki et al., 2001b). Although the 5S rRNA, which is one of the main structural components of the CP in the bacterial LSU (Ban et al., 2000), is absent in the mitoribosome, the CP itself in the mitoribosome is almost twice as large. About 50% of the 5S rRNA mass is replaced here by proteins (Figure 5). Our map reveals a handlelike cylindrical structure on the solvent side of the LSU, whose two ends connect to the CP and the main body. We designate this structure the LSU handle (LH in Figures 1A and 5C). This protein structure is oriented such that it would, in a bacterial ribosome, lie parallel to helices 4 and 5 of the 5S rRNA (see Ban et al., 2000; Figure 5E). Possibly, the LSU handle assumes some of the roles of the 5S rRNA in the mitoribosome. As compared to the mitoribosomal SSU, a larger proportion (28%) of the missing bacterial rRNA segments in the LSU is replaced by proteins (also see Supplemental Figure S1B).

Twenty-eight of the mitoribosome LSU proteins show sequence homology to their bacterial counterparts. With the exception of proteins L2 and L4, these homologs are significantly larger than their bacterial counterparts (Koc et al., 2001b; Suzuki et al., 2001b). The mitoribosome LSU possesses 20 additional proteins that are each 12–60 kDa in size. Most of the peripheral regions of the LSU are porous and are built up of mitoribosome-specific proteins, including extensions to the homolog proteins (Figure 5C). The bulk of the additional protein mass is found at the CP, on the solvent side, and in the lower-body regions near domains III and VI of the LSU rRNA (Ban et al., 2000). Bacterial proteins L5, L6, L25, L26, L29, and L31 are absent in the mitoribosome. Of these, a major portion of protein L5, which is known to interact with the 5S rRNA in the CP and which forms B1 group bridges with the SSU, and protein L29, which is one of the proteins that encircles the polypeptide exit tunnel in the bacterial ribosome (Nissen et al., 2000), are structurally compensated by mitoribosome-specific proteins. While the position of protein L6 is only partially compensated, the positions of L25 and L31 are left almost completely unfilled.

Figure 5. Structural Analysis of the LSU of the Mitoribosome

(A) Secondary structure diagram of the bovine mitochondrial 16S rRNA (purple) superimposed on that of the bacterial 23S rRNA. RNA regions absent in the mitoribosome thus appear black. Roman numerals identify the six domains of the rRNA, and helices are identified by the adjacent numbers. Four parallel purple lines in the domain I region indicate a small segment of rRNA for which no secondary structure information is available.

(B) Stereo representation of the fitting of conserved domains (ribbons) into the cryo-EM map of the mitoribosome LSU shown from its interface side. rRNA components were taken from the crystallographic structures of the *Deinococcus radiodurans* (Harms et al., 2001; PDB ID 1KC9) and *Haloarcula marismortui* (Ban et al., 2000; PDB ID 1FFK) 50S LSUs, and structures of homologous proteins were taken from the crystallographic maps of the *D. radiodurans* and *T. thermophilus* (Yusupov et al., 2001; PDB ID 1G1Y) 50S LSUs. The conserved structural components (pinkish purple, rRNA; green, homologous proteins) are shown as translucent surfaces, while the mitoribosome-specific proteins are shown as solid blue surfaces.

(C) Stereo representation of the fitting, as in (B), but shown from the solvent side, i.e., rotated relative to (B) by $\sim 180^{\circ}$ around a vertical axis.

(D and E) Superposition of the nonconserved domains from the crystallographic structure of the bacterial LSUs (black ribbons, rRNA; gray ribbons, proteins) onto the LSU map (solid surfaces) shown in views similar to those in (B) and (C). The uncompensated portion of the 5S rRNA can also be seen (colored gold) in (E). Small patches colored in yellow, dark blue (only minutely visible on CP, behind LH in [E]), and maroon (only minutely visible on CP in [D]) correspond to protein masses that compensate, respectively, for missing segments of bacterial 23S rRNA, 5S rRNA, and proteins. Thus, the blue in (D) and (E) represents the protein masses that do not compensate for any missing bacterial ribosomal components. Unlike the SSU, a significant number of compensated masses are embedded in the core of the LSU structure (not visible here, but see Supplemental Figure S1B). Landmarks: numbers prefixed "L" identify the LSU proteins; numbers prefixed "H" identify the LSU rRNA helices; D I, missing segments of domain I helices; D III, missing segments of domain III helices. All other landmarks are as in Figures 1 and 2.

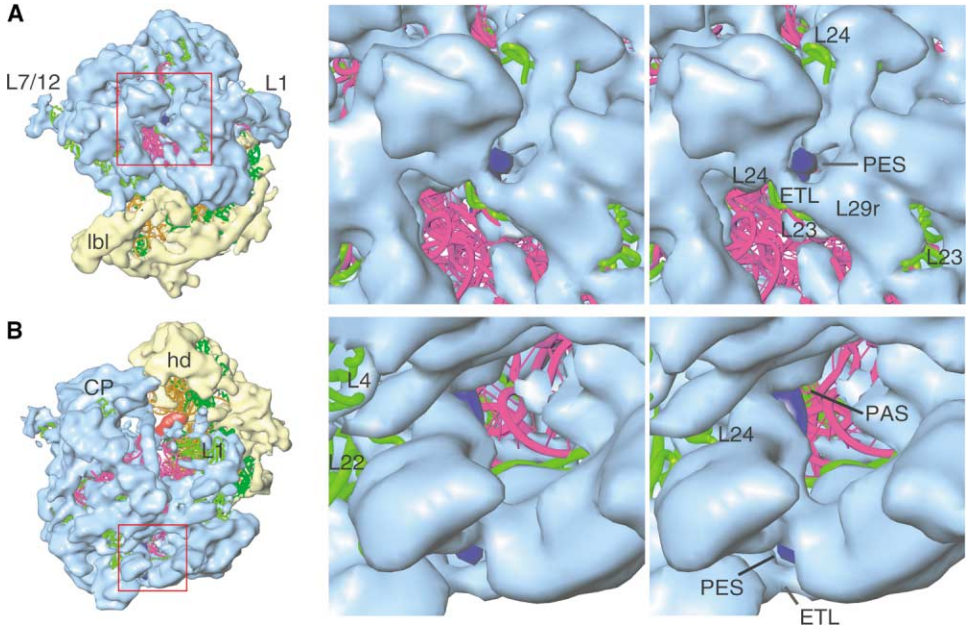

Figure 6. Stereo Representations of the Topographies of the Two Putative Sites of Polypeptide Exit in the LSU of the Mitoribosome

(A) The polypeptide exit site (PES) of the polypeptide exit tunnel, as seen from the bottom of the LSU.

(B) The LSU is shown from the L1 protein side to reveal a large opening (PAS) in the tunnel before the PES. The orientations of the 55S mitoribosome, with the area boxed in red enlarged for the stereo depiction, are shown in the corresponding panels to the left. A model of an α-helical polypeptide chain (dark blue) is used to delineate the polypeptide exit tunnel (also see Figure 7A). Landmarks: PAS, polypeptide-accessible site; ETL, exit tunnel lid; L29r, a mitoribosome-specific protein that replaces the bacterial protein L29. Segments of LSU proteins (green) present in the immediate vicinity are identified. All other landmarks are as in previous figures.

The Polypeptide Exit Tunnel

Newly synthesized nascent polypeptide chains emerge from the ribosome through a tunnel-like feature, the polypeptide exit tunnel. This tunnel connects the peptidyl-transferase center, the site of peptide bond formation, to the exterior of the ribosome, where nascent chains emerge through the polypeptide exit site (Figures 6 and 7A). The structural organization of the exit tunnel in cytoplasmic ribosomes has been studied by both cryo-EM (Frank et al., 1995; Beckmann et al., 2001; Gabashvili et al., 2001) and X-ray crystallography (Nissen et al., 2000). However, the tunnel revealed in our cryo-EM map of the mitoribosome is distinctly different in structure from the tunnels in the cytoplasmic ribosomes. In the mitoribosome, the tunnel has a wide opening well before the conventional polypeptide exit site (PES in Figures 6 and 7A). This site of premature exposure is located about 63 Å from the peptidyl-transferase center and allows free access to the solvent. Therefore, we designate this opening as the polypeptide-accessible site (PAS in Figures 6B and 7A; also see Supplemental Movie S1). Possibly, some of the nascent chains that are being synthesized on the mitoribosome emerge from the ribosome through this accessible site rather than being routed all the way through to the conventional exit site, ~88 Å from the peptidyl-transferase center. Thus, two pathways may exist by which nascent chains can emerge from the mitoribosome, perhaps allowing alternative interactions with different classes of chaperones involved in the assembly of the large oligomeric complexes of which they are components.

As noted earlier, protein L29 and the majority of domains I and III of the bacterial 23S rRNA are absent in the mitoribosome. These are the components of the polypeptide exit tunnel in the bacterial ribosome (Nissen et al., 2000). The other LSU proteins, L22, L23, and L24, which together with L29 surround the exit site of the tunnel in the bacterial ribosome, are represented by much larger homologs in the mitoribosome (Koc et al., 2001b; Suzuki et al., 2001b). However, because of the absence of 23S rRNA domains I and III, domains which together form the inner lining of most of the solvent side of the tunnel in the bacterial ribosome, the structure of the lower two-thirds of the tunnel in the mitoribosome is drastically different and is composed mainly of mitoribosome-specific proteins (Figure 7A). Since the majority of the rRNA domain I (Figure 5E) and a significant portion of domain III (Figure 5D) are not replaced by proteins, a wide opening is created (PAS in Figure 6B), and the overall structure of the tunnel is more open to the solvent. Furthermore, the conventional polypeptide exit site is surrounded by mitoribosome-specific proteins and is partially covered by a lidlike structure (exit tunnel lid [ETL] in Figure 6), which appears to be formed by a protrusion of a large protein that replaces the bacterial protein L29 in the mitoribosome.

In contrast to the variety of possible destinations for the polypeptides synthesized by cytoplasmic ribosomes, all of the polypeptides synthesized by mitoribosomes are inserted into the inner mitochondrial membrane. Although it is not yet clear whether polypeptides are inserted cotranslationally into the membrane, current evidence indicates this is most likely the case (see Stuart, 2002). The Oxa1 family of proteins, which are

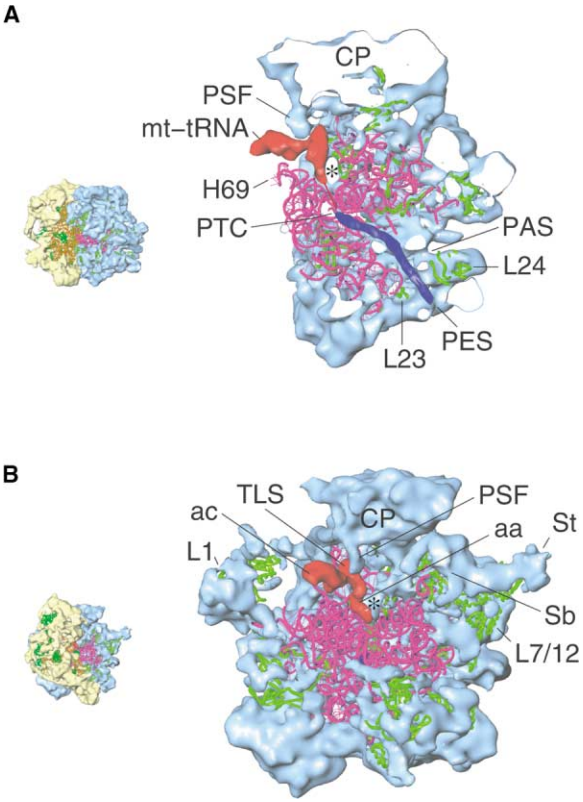

Figure 7. Topology of the Polypeptide Exit Tunnel and Interactions of the mt tRNA (red) with the LSU of the Mitoribosome

(A) Cut-away view of the LSU. A portion of the LSU structure has been computationally removed (white surfaces correspond to the cutting plane) from the side toward the viewer to reveal the tunnel topology. An α-helical polypeptide chain (dark blue) has been docked into the tunnel and filtered to the resolution of the cryo-EM map.

(B) The LSU is shown from the interface side in a view similar to that in Figure 5B. The mt tRNA interacts with two mitoribosome-specific proteins, one identified as the P site finger (PSF) and one denoted with an asterisk (*). The orientations of the 55S mitoribosome are shown in the corresponding panels as thumbnails to the left. Landmarks: PTC, peptidyl-transferase center; aa, acceptor arm of the mt tRNA; ac, anticodon end of the mt tRNA; TLS, T loop side of the mt tRNA. All remaining landmarks are as in previous figures.

members of the conserved YidC/Alb3 protein family (known to facilitate the insertion of polypeptide chains into membranes), have been localized to the inner membrane of yeast mitochondria (Stuart, 2002). Recent studies have suggested that proteins of the Oxa1 family interact with the nascent chain while it is still being synthesized on the mitoribosome (Hell et al., 2001). Interestingly, the N-terminal domains of the some of the mitochondrially synthesized polypeptides, whose insertion is facilitated by proteins of the Oxa1 family, remain in the matrix of the mitochondrion. We speculate that the N-terminal domains of the nascent chains are held by proteins of the Oxa1 family by their interaction with the mitoribosome at the polypeptide-accessible site, while the rest of the polypeptide is cotranslationally inserted into the membrane through the conventional exit site. To this end, the lid-like structure at the exit site could help to regulate the release of the nascent chain and could assist in the formation of loops after successive insertions of the transmembrane domains.

Interactions of the P Site Bound Mitochondrial tRNA with the Mitoribosomal Proteins

Strikingly, the mitoribosome purifies with a tRNA bound to the P site (Figure 1A). The mitoribosome LSU possesses a unique finger-like structure, the P site finger (PSF in Figures 1A, 2A, 2D, 5B, and 7), a protein that extends from the CP and that interacts with the P site bound mt tRNA. This interaction involves the T loop side (TLS in Figure 7B) of the mt tRNA, which is a well-defined structure in our map. Docking of the crystallographic structure of a cytoplasmic tRNA (Basavappa and Sigler, 1991) into the cryo-EM map produces a very good overall fit (not shown), except in the elbow region involving the anticodon-arm side. Our map apparently shows an averaged structure for the mammalian mt tRNAs, some of which are known to have unusually small T loops (e.g., Hanada et al., 2001; Ohtsuki et al., 2002). Possibly, the P site finger complements the smaller T loops in the mt tRNAs. The lower CCA arm of the mt tRNA interacts with another protein (asterisk in Figure 7). It is likely that these interactions stabilize the binding of the mt tRNA in the P site and that they are involved in regulating the movement of tRNAs (Agrawal et al., 2000) on the mitoribosome. Such an additional stabilization of the mt tRNA by mitoribosomal proteins could be one of the reasons why the purification of the mitoribosome resulted in the copurification of a strongly bound tRNA at the P site. Our finding of a strongly bound P site tRNA is in contrast to the characteristic state of the bacterial ribosome, which purifies with a strongly bound tRNA at the E site (Remme et al., 1989; Agrawal et al., 2000; Cate et al., 1999). Interestingly, many rRNA residues involved in the binding of tRNA at the bacterial E site (Yusupov et al., 2001) (for example, helices 11 and 68 and a portion of the loop between helices 76 and 77) are absent in the LSU of the mitoribosome (Figure 5A). The strong binding of the P site tRNA suggests that the E site is very weak or even nonexistent in the mitoribosome, as was implied in a recent phylogenetic study (Mears et al., 2002).

Conclusions

The study presented here describes the first structure, to our knowledge, determined for an organellar ribosome. Through molecular analysis of the cryo-EM map, we have answered the long-standing question of whether the truncated regions of the rRNA are compensated by the presence of additional and enlarged proteins in the mitoribosome. In contrast to what has been generally believed, our study provides direct evidence that the enlarged and additional proteins present in the mitoribosome do not necessarily compensate for the majority of the missing rRNA segments. Instead, many of them occupy new quaternary positions in both subunits of the mitoribosome. Furthermore, we have derived the positions and shapes of the masses corresponding to the mitoribosome-specific proteins, together with the extensions to the proteins that are bacterial homologs. The next challenge will be to assign these masses to particular proteins. A combination of immuno-EM and

homology-modeling studies, making use of the cryo-EM map, could be utilized to identify all of the mitoribosome-specific proteins and to generate a near-atomic resolution model of the mitoribosome. While our analysis gives no indication of the presence of any proteins either in the decoding site of the SSU or in the peptidyl-transferase center of the LSU, the limited resolution prevents us from ruling out the possibility that a strand of polypeptide chain reaches closer to these functional centers in the mitoribosome. Distinct topological differences in the mRNA entry and polypeptide exit sites, as compared to the corresponding regions in cytoplasmic ribosomes, suggest mechanistic divergence of protein synthesis on the mitoribosome. Further structural and functional characterization of the protein components present at these sites will be the key to establishing a detailed mechanism for the recruitment of the mt mRNAs to the mitoribosome and for the insertion of the nascent chains into the inner mitochondrial membrane.

Experimental Procedures

Isolation of the Mammalian Mitochondrial Ribosomes

Bos taurus mitochondria and 55S ribosomes were prepared as described previously (Matthews et al., 1982). The 55S tight couples were subsequently isolated on 10%–30% sucrose gradients in 50 mM Tris-HCl (pH 7.6), 40 mM KCl, 20 mM $MgCl_2$, and 1 mM dithiothreitol. Ribosomes were collected by centrifugation at 140,000 × g for 6 hr in a Beckman Type 50 rotor; resuspended in buffer containing 20 mM Tris-HCl (pH 7.6), 40 mM KCl, 20 mM $MgCl_2$, 10% glycerol, and 1 mM dithiothreitol; and fast-frozen in small aliquots for storage at −70°C.

Cryo-Electron Microscopy and Three-Dimensional Image Reconstruction

Cryo-EM grids were prepared according to standard procedures (Wagenknecht et al., 1988). Data were collected on a Philips FEI (Eindhoven, The Netherlands) Tecnai F20 field emission gun electron microscope equipped with low-dose kit and an Oxford cryo-transfer holder at a magnification of 50,000×. 194 micrographs were scanned on a Zeiss flatbed scanner (Z/I Imaging Corporation, Huntsville, AL) with a step size of 14 μm, corresponding to 2.82 Å on the object scale. Because of their greater proportion of protein (O'Brien et al., 1990; O'Brien, 2002), mitoribosomes are much more labile than are cytoplasmic ribosomes, and their cryo-EM images have poorer contrast at low defocus values. In addition, three isoforms of protein S18 (ranging from 11.8 to 26.5 KDa in size) may be present in ribosomes of even a single mitochondrion (Koc et al., 2001b). The low contrast of the images and this inherent conformational heterogeneity both pose difficulties in the acquisition of a high-resolution 3D cryo-EM map for the mitoribosome. The projection-matching procedure (Penczek et al., 1994) within the SPIDER software (Frank et al., 2000) was used to obtain the 3D map. Since the mitoribosome was expected to display overall morphological similarity to the bacterial ribosome (see Introduction), we initially used an 11.5 Å resolution *E. coli* 70S ribosome map (Gabashvili et al., 2000) as the reference to obtain a low-resolution map of the mitoribosome from about 3000 cryo-EM images of individual mitoribosomes. The mitoribosome 3D map so obtained was used as reference for the alignment of the larger data set. Initially, 93,908 images, sorted into 30 groups according to defocus value (ranging from 1.4–4.4 μm), were picked. Because of the problem of conformational heterogeneity, we had to eliminate a large portion of the data set in order to achieve high resolution. From the pool of 93,908 images, only 35,759 were retained after manual screening and removal of images from overrepresented groups within 83 equispaced views of the ribosome. Further screening of this set of images, based on ranking of crosscorrelation coefficients, eliminated another 6156 images. A total of 29,603 images were thus included in the final 3D reconstruction. The resolution of the final CTF-corrected 3D map, estimated using the Fourier shell correlation with a cutoff value of 0.5 (see Gabashvili et al., 2000), was 13.5 Å (or 9.1 Å by the 3σ criterion [Orlova et al., 1997]). The falloff of the Fourier amplitudes toward higher spatial frequencies was corrected as described previously (Gabashvili et al., 2000), using the X-ray solution scattering intensity distribution of the *E. coli* 70S ribosome. RNA and protein components of the 55S mitoribosome map were computationally separated using a method (Spahn et al., 2000) based on differences in the density distribution of the two moieties, taking into account the molecular masses and contiguity constraints. Visualization and interpretation of the map and docking of crystallographic structures were performed using SPIDER, IRIS Explorer (Numerical Algorithms group, Inc., Downers Grove, IL), O (Jones et al., 1991), and Ribbons (Carson, 1991).

Acknowledgments

We thank Arunasree Silasagaram for assistance with image processing; Paul Templeton for help in the preparation of mitoribosomes; Michael Watters for help with some of the illustrations; Joachim Frank, Carmen Mannella, and Chandana Barat for helpful comments; and Adriana Verschoor for invaluable suggestions and critical readings of the manuscript. This work was supported, in part, by grants from the National Institutes of Health, GM61576 (to R.K.A.) and GM32734 (to L.L.S.), and from the Human Frontier Science Program, RGY232003 (to R.K.A.).

Received: June 12, 2003
Revised: September 5, 2003
Accepted: September 15, 2003
Published: October 2, 2003

References

Agrawal, R.K., Penczek, P., Grassucci, R.A., and Frank, J. (1998). Visualization of elongation factor G on the *Escherichia coli* ribosome: the mechanism of translocation. Proc. Natl. Acad. Sci. USA *95*, 6134–6138.

Agrawal, R.K., Spahn, C.M., Penczek, P., Grassucci, R.A., Nierhaus, K.H., and Frank, J. (2000). Visualization of tRNA movements on the *Escherichia coli* 70S ribosome during the elongation cycle. J. Cell Biol. *150*, 447–459.

Anderson, S., de Brujjn, M., Coulson, A., Eperon, I., Sanger, F., and Young, I. (1982). Complete sequence of bovine mitochondrial DNA: conserved features of the mammalian mitochondrial genome. J. Mol. Biol. *156*, 683–717.

Attardi, G. (1985). Animal mitochondrial DNA: an extreme example of genetic economy. Int. Rev. Cytol. *93*, 93–145.

Ban, N., Nissen, P., Hansen, J., Moore, P.B., and Steitz, T.A. (2000). The complete atomic structure of the large ribosomal subunit at 2.4 Å resolution. Science *289*, 905–920.

Basavappa, R., and Sigler, P.B. (1991). The 3 Å crystal structure of yeast initiator tRNA: functional implications in initiator/elongator discrimination. EMBO J. *10*, 3105–3111.

Beckmann, R., Spahn, C.M., Eswar, N., Helmers, J., Penczek, P.A., Sali, A., Frank, J., and Blobel, G. (2001). Architecture of the protein-conducting channel associated with the translating 80S ribosome. Cell *107*, 361–372.

Brenner, C., and Kroener, G. (2000). Mitochondria—the death signal. Science *289*, 1150–1151.

Cannone, J.J., Subramanian, S., Schnare, M.N., Collett, J.R., D'Souza, L.M., Du, Y., Feng, B., Lin, N., Madabusi, L.V., Mueller, K.M., et al. (2002). The Comparative RNA Web (CRW) Site: an online database of comparative sequence and structure information for ribosomal, intron, and other RNAs. BMC Bioinformatics *3*, 2.

Carson, M. (1991). Ribbons 2.0. J. Appl. Crystallogr. *24*, 103–106.

Cate, J.H., Yusupov, M.M., Yusupova, G.Z., Earnest, T.N., and Noller, H.F. (1999). X-ray crystal structures of 70S ribosome functional complexes. Science *285*, 2095–2104.

Chomyn, A., Cleeter, M.W., Ragan, C.I., Riley, M., Doolittle, R.F., and Attardi, G. (1986). URF6, last unidentified reading frame of human

mtDNA, codes for an NADH dehydrogenase subunit. Science *234*, 614–618.

Dube, P., Bacher, G., Stark, H., Mueller, F., Zemlin, F., van Heel, M., and Brimacombe, R. (1998). Correlation of the expansion segments in mammalian rRNA with the fine structure of the 80 S ribosome; a cryoelectron microscopic reconstruction of the rabbit reticulocyte ribosome at 21 Å resolution. J. Mol. Biol. *279*, 403–421.

Frank, J., and Agrawal, R.K. (2000). A ratchet-like inter-subunit reorganization of ribosome during translocation. Nature *406*, 318–322.

Frank, J., and Agrawal, R.K. (2001). Ratchet-like movements between the two ribosomal subunits: their implications in elongation factor recognition and tRNA translocation. Cold Spring Harb. Symp. Quant. Biol. *66*, 67–75.

Frank, J., Zhu, J., Penczek, P., Li, Y., Srivastava, S., Verschoor, A., Radermacher, M., Grassucci, R., Lata, K.R., and Agrawal, R.K. (1995). A model of protein synthesis based on cryo-electron microscopy of the *E. coli* ribosome. Nature *376*, 441–444.

Frank, J., Penczek, P., Agrawal, R.K., Grassucci, R.A., and Heagle, A.B. (2000). Three-dimensional cryoelectron microscopy of ribosomes. Methods Enzymol. *317*, 276–291.

Gabashvili, I.S., Agrawal, R.K., Spahn, C.M., Grassucci, R., Svergun, D., Frank, J., and Penczek, P. (2000). Solution structure of the *E. coli* 70S ribosome at 11.5 Å resolution. Cell *100*, 537–549.

Gabashvili, I.S., Gregory, S.T., Valle, M., Grassucci, R., Worbs, M., Wahl, M.C., Dahlberg, A.E., and Frank, J. (2001). The polypeptide tunnel system in the ribosome and its gating in erythromycin resistance mutants of L4 and L22. Mol. Cell *8*, 181–188.

Gomez-Lorenzo, M.G., Spahn, C.M., Agrawal, R.K., Grassucci, R.A., Penczek, P., Chakraburtty, K., Ballesta, J.P., Lavandera, J.L., Garcia-Bustos, J.F., and Frank, J. (2000). Three-dimensional cryo-electron microscopy localization of EF2 in the *Saccharomyces cerevisiae* 80S ribosome at 17.5 Å resolution. EMBO J. *19*, 2710–2718.

Gray, M.W., Burger, G., and Lang, B.F. (2001). The origin and early evolution of mitochondria. Genome Biol. *2,* 1018.1–1018.5.

Hanada, T., Suzuki, T., Yokogawa, T., Takemoto-Hori, C., Sprinzl, M., and Watanabe, K. (2001). Translation ability of mitochondrial $tRNAs^{Ser}$ with unusual secondary structures in an in vivo translation system of bovine mitochondria. Genes Cells *6*, 1019–1030.

Harms, J., Schluenzen, F., Zarivach, R., Bashan, A., Gat, S., Agmon, I., Bartels, H., Franceschi, F., and Yonath, A. (2001). High resolution structure of the large ribosomal subunit from a mesophilic eubacterium. Cell *107*, 679–688.

Hell, K., Neupert, W., and Stuart, R.A. (2001). Oxa1p acts as a general membrane insertion machinery for proteins encoded by mitochondrial DNA. EMBO J. *20*, 1281–1288.

Jones, T.A., Zou, J.Y., Cowan, S.W., and Kjeldgaard. (1991). Improved methods for building protein models in electron density maps and the location of errors in these models. Acta Crystallogr. A *47*, 110–119.

Koc, E.C., Burkhart, W., Blackburn, K., Moseley, A., Koc, H., and Spremulli, L.L. (2000). A proteomics approach to the identification of mammalian mitochondrial small subunit ribosomal proteins. J. Biol. Chem. *275*, 32585–32591.

Koc, E.C., Ranasinghe, A., Burkhart, W., Blackburn, K., Koc, H., Moseley, A., and Spremulli, L.L. (2001a). A new face on apoptosis: death-associated protein 3 and CDPD9 are mitochondrial ribosomal proteins. FEBS Lett. *492*, 166–170.

Koc, E.C., Burkhart, W., Blackburn, K., Moyer, M.B., Schlatzer, D.M., Moseley, A., and Spremulli, L.L. (2001b). The large subunit of the mammalian mitochondrial ribosome. Analysis of the complement of ribosomal proteins present. J. Biol. Chem. *276*, 43958–43969.

Matthews, D.E., Hessler, R.A., Denslow, N.D., Edwards, J.S., and O'Brien, T.W. (1982). Protein composition of the bovine mitochondrial ribosome. J. Biol. Chem. *257*, 8788–8794.

Mears, J.A., Cannone, J.J., Stagg, S.M., Gutell, R.R., Agrawal, R.K., and Harvey, S.C. (2002). Modeling a minimal ribosome based on comparative sequence analysis. J. Mol. Biol. *321*, 215–234.

Nissen, P., Hansen, J., Ban, N., Moore, P.B., and Steitz, T.A. (2000). The structural basis of ribosome activity in peptide bond synthesis. Science *289*, 920–930.

O'Brien, T.W. (1971). The general occurrence of 55 S ribosomes in mammalian liver mitochondria. J. Biol. Chem. *246*, 3409–3417.

O'Brien, T.W. (2002). Evolution of a protein-rich mitochondrial ribosome: implications for human genetic disease. Gene *286*, 73–79.

O'Brien, T.W., Denslow, N.D., Anders, J., and Courtney, B. (1990). The translation system of mammalian mitochondria. Biochim. Biophys. Acta *1050*, 174–178.

O'Brien, T.W., Liu, J., Sylvester, J., Mourgey, E.B., Fischel-Ghodsian, N., Thiede, B., Wittmann-Liebold, B., and Graack, H.-R. (2000). Mammalian mitochondrial ribosomal proteins (4): amino acid sequencing, characterization and identification of corresponding gene sequences. J. Biol. Chem. *275*, 18153–18159.

Ohtsuki, T., Kawai, G., and Watanabe, K. (2002). The minimal tRNA: unique structure of Ascaris suum mitochondrial tRNA(Ser)(UCU) having a short T arm and lacking the entire D arm. FEBS Lett. *514*, 37–43.

Ojala, D.K., Montoya, J., and Attardi, G. (1980). The putative mRNA for subunit II of human cytochrome c oxidase starts directly at the translation initiator codon. Nature *287*, 79–82.

Orlova, E.V., Dube, P., Harris, J.R., Beckman, E., Zemlin, F., Markl, J., and van Heel, M. (1997). Structure of keyhole limpet hemocyanin type 1 (KHL1) at 15 Å resolution by electron cryomicroscopy and angular reconstruction. J. Mol. Biol. *271*, 417–437.

Patel, V.B., Cunningham, C.C., and Hantgan, R.R. (2001). Physiochemical properties of rat liver mitochondrial ribosomes. J. Biol. Chem. *276*, 6739–6746.

Penczek, P., Grassucci, R.A., and Frank, J. (1994). The ribosome at improved resolution: new techniques for merging and orientation refinement in 3D cryo-electron microscopy of biological particles. Ultramicroscopy *53*, 251–270.

Remme, J., Morgus, T., Villems, R., and Nierhaus, K.H. (1989). The third ribosomal tRNA-binding site, the E site, is occupied in native polysomes. Eur. J. Biochem. *183*, 281–284.

Spahn, C.M.T., Penczek, P.A., Leith, A., and Frank, J. (2000). A method for differentiating proteins from nucleic acids in intermediate-resolution density maps: cryo-electron microscopy defines the quaternary structure of the *Escherichia coli* 70S ribosome. Structure *8*, 937–948.

Spahn, C.M.T., Beckmann, R., Eswar, N., Penczek, P.A., Sali, A., Blobel, G., and Frank, J. (2001). Structure of the 80S ribosome from *Saccharomyces cerevisiae*: tRNA-ribosome and subunit-subunit interactions. Cell *107*, 373–386.

Stark, H., Rodnina, M., Rinke-Appel, J., Brimacombe, R., Wintermeyer, W., and van Heel, M. (1997). Visualization of elongation factor Tu on the *Escherichia coli* ribosome. Nature *389*, 403–406.

Stuart, R.A. (2002). Insertion of proteins into inner membrane of mitochondria: the role of the Oxa1 complex. Biochim. Biophys. Acta *1592*, 79–87.

Suzuki, T., Terasaki, M., Takemoto-Hori, C., Hanada, T., Ueda, T., Wada, A., and Watanabe, K. (2001a). Proteomic analysis of the mammalian mitochondrial ribosome. Identification of protein components in the 28S small subunit. J. Biol. Chem. *276*, 33181–33195.

Suzuki, T., Terasaki, M., Takemoto-Hori, C., Hanada, T., Ueda, T., Wada, A., and Watanabe, K. (2001b). Structural compensation for the deficit of rRNA with proteins in the mammalian mitochondrial ribosome. Systematic analysis of protein components of the large ribosomal subunit from mammalian mitochondria. J. Biol. Chem. *276*, 21724–21736.

Valle, M., Sengupta, J., Swami, N.K., Grassucci, R.A., Burkhardt, N., Nierhaus, K.H., Agrawal, R.K., and Frank, J. (2002). Cryo-EM reveals an active role for aminoacyl-tRNA in the accommodation process. EMBO J. *21*, 3557–3567.

Wagenknecht, T., Grassucci, R., and Frank, J. (1988). Electron microscopy and computer image averaging of ice-embedded large ribosomal subunits from *Escherichia coli*. J. Mol. Biol. *199*, 137–145.

Wimberly, B.T., Brodersen, D.E., Clemons, W.M., Morgan-Warren,

R.J., Carter, A.P., Vonrhein, C., Hartsch, T., and Ramakrishnan, V.R. (2000). Structure of the 30S ribosomal subunit. Nature *407*, 327–339.

Wittmann-Liebold, B. (1985). Ribosomal proteins: their structure and evolution. In Structure, Function, and Genetics of Ribosomes, B. Hardesty, and G. Kramer, eds. (New York: Springer-Verlag) pp. 326–361.

Wolstenholme, D. (1992). Animal mitochondrial DNA: structure and evolution. In Mitochondrial Genomes, D. Wolstenholme, and K. Jeon, eds. (New York: Academic Press) pp. 173–216.

Yusupov, M.M., Yusupova, G.Z., Baucom, A., Lieberman, K., Earnest, T.N., Cate, J.H., and Noller, H.F. (2001). Crystal structure of the ribosome at 5.5 Å resolution. Science *292*, 883–896.

Yusupova, G.Z., Yusupov, M.M., Cate, J.H., and Noller, H.F. (2001). The path of messenger RNA through the ribosome. Cell *106*, 233–241.